International Journal of New Horizons in Physics

http://dx.doi.org/10.12785/ijnhp/020202

Microstructural and electrical characteristics of sprayed Tungsten oxide thin films

S. A. Aly, A. A. Akl, and D. H. Mahmoud

Physics Department, Faculty of Science, Minia University, Minia, Egypt

Received: 02 Jul. 2014, Revised: 20 Oct. 2014, Accepted: 09 Nov. 2014
Published online: 01 Jul. 2015

Abstract: In this work, tungsten oxide thin films were grown on preheated glass substrates by spray pyrolysis technique. The microstructure and electrical properties of the prepared samples were studied. The influence of post deposition thermal annealing on the crystallization of prepared films has been investigated. X-ray diffraction (XRD) confirmed that all samples prepared at different deposition temperatures, $T_{dep} \leq 350^{\circ}$C, are almost in the amorphous form, while sample deposited at $T_{dep} = 400^{\circ}$C possess hexagonal structures with a preferential orientation along (200) direction. Moreover, the degree of crystallinity was improved by thermal annealing. The microstructural parameters (crystallite size and microstrain) were determined using Sherrer's formula measurements of FWHM of the characterized peaks. The dark electrical resistivity at different deposition temperatures, T_{dep} was measured at room temperature. The value of activation energy is calculated and is found to be ranged from 0.79-0.89 eV depending on the annealing temperature.

Keywords: Thin films, Annealing temperature, Spray pyrolysis, Tungsten oxide, X-ray diffraction, Electrical properties.

1 Introduction

A transition metal oxide has extracted extensive interest over recent years due to its numerous outstanding properties, such as photochromic and thermochromic properties [1,2,3,4]. There has been a great interest in studying electrical properties of thin films of these materials.

Nowadays, owing to the extraordinary properties in extreme conditions, WO_3 thin films also plays a key role in the field of solar energy control coatings for automotive antidazzle rearview mirrors, optical displays and smart windows [5,6,7,8]. When WO_3 films are used on the smart windows as the primary materials, they can adjust the room temperature by responding to the variation of the brightness of the environment, dynamically Modulating the optical transmittance [9,10]. Films prepared by different methods exhibit different crystal structure, morphology, pore structure and specific surface area. Because of its high sensitivity to many kinds of gases, such as O_3 [11], O_2 [12], NO_2 [13], NO, NH_3, H_2S [14], H_2 [15,16] and ethanol [17]. WO_3 received much attention in recent years.

Recently it has been reported that WO3 was used for the fabrication of multifunctional sensors [18], which opens a new way for the application of WO_3 thin films. The sensing mechanism of the sensor lies in the change of thin film resistance resulting from physisorption, chemisorption and catalytic reactions of gas-phase species with the film surface [19].

Various deposition techniques, such as thermal evaporation [20,21], spray pyrolysis [22], sputtering [23], pulsed laser ablation [24], sol-gel coating [25] and chemical vapor deposition [26] have been used for deposition of WO_3thin films. The aims of the present work has to three fold the first is an investigation of the effect of deposition temperature, T_{dep} and annealing temperature, T_{ann}, on the crystalline growth of microstructural parameters both crystallite size and microstrain of tungsten oxide films deposited by spray pyrolysis method, the second is studying the electrical resistivety as well as activation energy of the films and the third is interpreting the change in electrical resistivity activation energy in terms of the change in microstructure parameters.

* Corresponding author e-mail:

© 2015 NSP
Natural Sciences Publishing Cor.

2 Experimental Details

2.1 Thin film deposition

Tungsten oxide samples of the same thickness ($\approx 650nm$) were deposited by spray pyrolysis technique (SPT) from ammonium para tungstate $((NH_4)_{10}(W_{12}O_{41})5H_2O)$ aqueous solution onto preheated glass substrate at temperatures 250, 300, 350 and 4000°C. The solution concentration was kept constant at 0.005 M for all samples and sprayed through a glass nozzle using air as a carrier gas onto the ultrasonically cleaned substrate. The resulting films were found to be uniform, adherent to the substrates, and slightly whitish in colour. In order to get homogeneous films, the height of the spraying nozzle and the rate of the spray were 40 cm and 4 ml / min, respectively and kept constant during spraying process. The film thicknesses were measured usingmechanical stylus method (MSM) (Sloan Dektak, model 11A) [27].

2.2 Characterization techniques

The structure characteristics of the films were studied using X-ray diffractometer (JEOL model JSDX- 60PA) with attached Ni-filtered $Cu-K_\alpha$ radiation (λ = 0.154184 nm). Continuous scanning was applied with a slow scanning speed (1o/min) and a small time constant (one second). Microstructure and the phase identification of the polycrystalline thin films of tungsten oxide at different annealing temperature, Tann were investigated. The crystallite size and microstrain of the films were determined using Sherrer's formula [28]. The average values of FWHM of the characterized peaks were measured after correction of instrumental factor. The DC of electrical resistivity measurement was performed on the films using by two-point probe technique at room temperature. Two aluminum electrodes were deposited on the tungsten oxide samples leaving an uncoated trip in the middle. The current-voltage characteristics were measured using Keithely digital electrometer (Model 616).

3 Results and discussion

3.1 Structural properties

3.1.1 Effect of deposition temperature

The XRD pattern was recorded for different films deposited onto glass substrates kept at different deposition temperatures, T_{dep}, the obtained results is depicted in Figure (1). The XRD results show that the structure is amorphous for all samples deposited at T_{dep}=250, 300 and 350°C, while sample deposited at T_{dep} = 400°C, is a polycrystalline WO_3 with a hexagonal structure. The presence of the characteristic lines corresponding to (100), (111), and (200) planes of WO_3 was observed and coincide with JCPDS Data file: 75?2187.

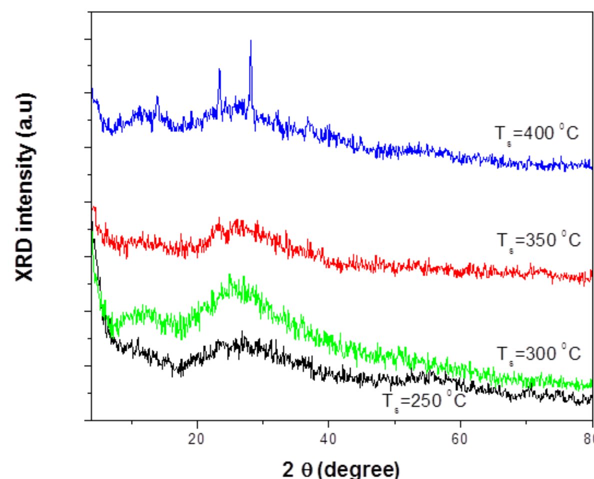

Fig. 1: XRD diffraction patterns of tungsten oxide samples at different deposition temperature, T_{dep}.

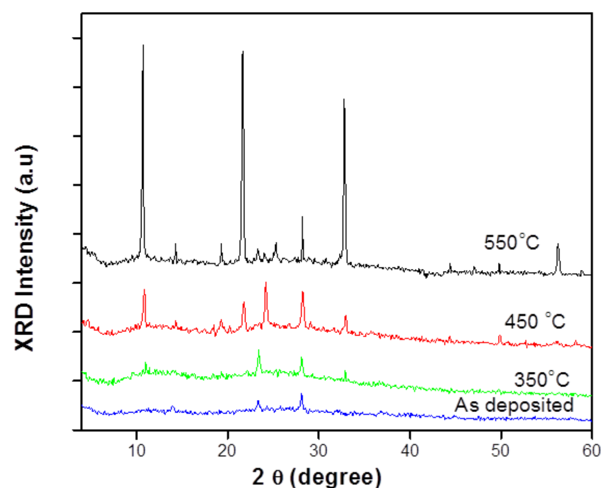

Fig. 2: XRD diffraction patterns of tungsten oxide samples at different annealing temperature, T_{ann}.

3.1.2 Effect of thermal annealing

Sample deposited at T_{dep} =400°C was subjected to post deposition annealing in air for a period of 2 hours at different T_{ann} (350, 450 and 550°C). The effect of

© 2015 NSP
Natural Sciences Publishing Cor.

Table 1: XRD pattern of sample prepared at T_{dep} = 400°C, then annealed for 2 hours in air at different T_{ann}.

2θ	As	deposited	Annealed	at 350°C	Annealed	at 400°C	Annealed	at 550°C	Identification	hkl
	d	$I/I_0\%$	d	$I/I_0\%$	d	$I/I_0\%$	d	$I/I_0\%$		
11.000	-	-	8.043	70	8.116	89	8.268	100	W_xO_{3-x}	
14.352	6.325	60	6.325	60	6.193	47	6.193	16	WO_3	(100)
19.362	-	-	4.598	60	4.598	45	4.598	15	W_xO_{3-x}	
21.800	-	-	4.040	63	4.076	48	4.076	97	W_xO_{3-x}	
23.314	3.801	80	3.801	100	3.817	45	3.817	14	WO_2	(111)
25.322	-	-	-	-	3.677	100	3.520	16	WO_3	(110)
28.205	3.175	100	3.175	90	3.153	86	3.164	27	WO_3	(200)
32.946	-	-	2.174	49	2.714	53	2.714	77	WO_2	(231)
44.443	-	-	-	-	2.040	26	2.040	8	WO_3	(211)
47.000	-	-	-	-	-	-	1.933	4	WO_3	(002)
49.802	-	-	-	-	1.827	28	1.831	8	WO_3	(220)
56.245	-	-	-	-	-	-	1.636	16	WO_3	(311)

post-deposition annealing on structure of the sample is shown in Figure (2). An increase in the peak intensity is appeared and evolution of other peaks appeared with increasing T_{ann}. The increase in the peaks intensity may be attributed to either the crystallite growth or the increase in the degree of crystallinity by increasing the temperature or both. Thus, annealing gives other phases as obtained in table 1. The table shows XRD pattern to d-values, directions and identification for the sample annealed at different annealing temperatures where there is a combination between two phases of WO_3 and WO_2 hexagonal and monoclinic structure respectively. The plane of (111) of WO_2 is observed from JCPDS Data file: 75?2187.

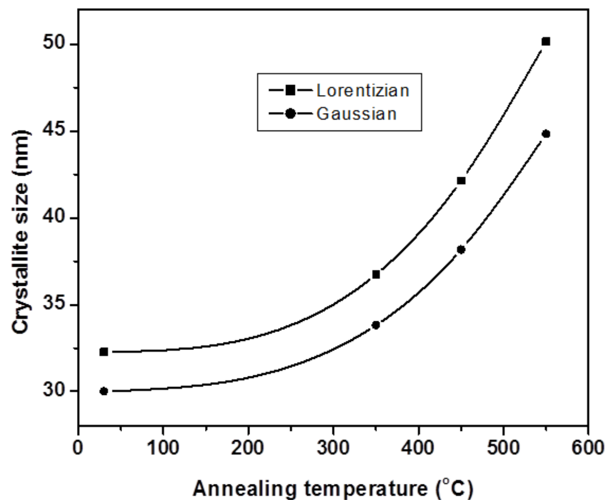

Fig. 3: The crystallite size as a function of annealing temperature.

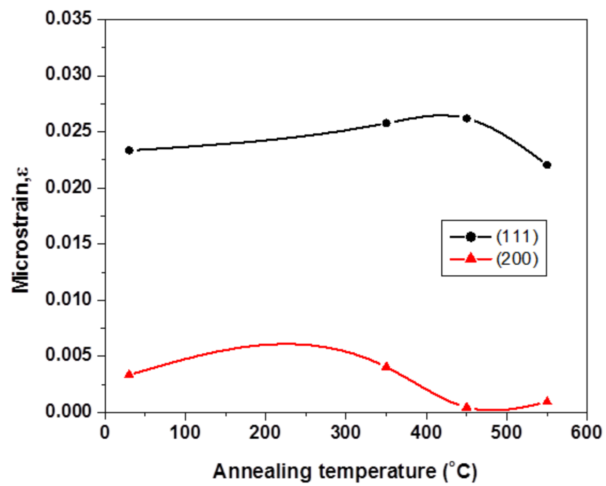

Fig. 4: The microstrain as a function of annealing temperature.

3.1.3 Nanostructure characteristics of WO_3 films

The microstructural parameters (crystallite/domain size and microstrain) of the prepared samples have been studied at different T_{ann}. The crystallite/ domain size is measured in the direction normal to the diffraction plane and consequently perpendicular to the substrate. Therefore, the observed increase in the crystallite/domain size may be interpreted in terms of a columnar grain growth. The microstrain is equivalent to a variation in interplanar spacing within domains by amount which depends on the elastic constants of the material and the nature of internal stresses. The Lorentzian (Cauchy) and Gaussian components of the integral breadth of pure specimen profile are given by

$$\beta_L = B - b \quad (1)$$

$$\beta_G^2 = B^2 - b^2 \quad (2)$$

© 2015 NSP
Natural Sciences Publishing Cor.

Where B and b are broadening and instrumental factor, respectively. The apparent crystallite/ domain size D is calculated from Sherrer's formula [28];

$$D = \frac{K\lambda}{\beta cos\theta} \quad (3)$$

where the constant K is taken to be 0.94, λ the wavelength of x-ray used which is $Cu - K_{\alpha}$ radiation (λ=0.154184nm), and β the full width at half maximum of the diffraction peaks The microstrain, ε in the film can be calculated from the following relation;

$$\varepsilon = \frac{\beta cos\theta}{4} \quad (4)$$

The variation of the crystallite size and microstrain of tungsten oxide sample with T_{ann} is depicted in Figure (3) and (4), respectively. It is evident that the crystallite size is increased gradually with raising T_{ann}. The increase in the crystallite size confirms the fact that the crystalline nature improved upon annealing. Increasing the crystallite size decreases the grain boundary area because of coalescence of smaller crystallite into larger one. Also, one can notice that the crystallite size calculated by Lorantzian is higher than that calculated by Gaussian. On the other hand, microstrain decreases at higher values of T_{ann}. Reduction of strain in the film due to some degree of reorientation of the particles at higher temperature. The micro-strain decreases after annealing expected to enhance the reduction in the concentration of lattice imperfections originating from lattice misfit in the film.

3.2 Electrical properties

3.2.1 Electrical resistivity

The dark electrical resistivity of the prepared samples was measured using the conventional two point probe technique assuming homogenous conduction throughout the film depth. Two aluminum electrodes have been deposited on the film to insure Ohmic contact with no Schottky. Figure(5) depicts the effect of deposition temperature, T_{dep}, on the electrical resistivity. A considerable decrease of the resistivity value is noticed with increasing deposition temperature up to 300°C) followed by a slight decrease up 400°C). The value of resistivity was found to be varied from $8.669x10^{7}$ to $7.196x10^{6}$ Ω.cm when T_{dep} varies from 250 to 400°C respectively. The general decrease of the resistivity with deposition temperature may be explained by assuming the two-phase model [7,29]. According to this model, the films material consists of nano-crystalline phase 30 nm crystallite size, dispersed in amorphous matrix. Elevating the deposition temperature causes the increase of the degree of crystallinity accompanied by increasing the number of crystallites rather than an increase of their size. This may explain the observed gradual decrease in the resistivity with the absence of a sharp amorphous-crystalline transformation.

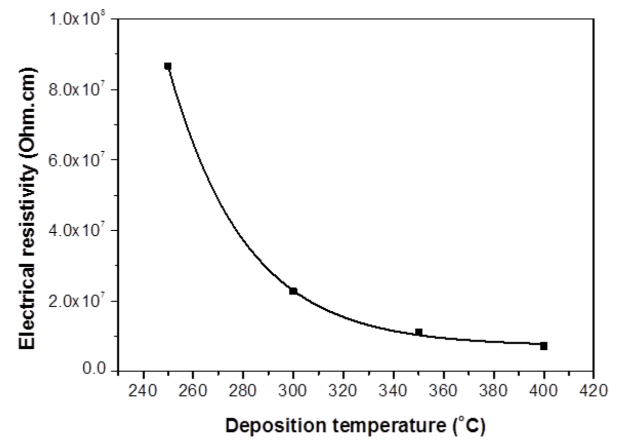

Fig. 5: Variation of electrical resistivity, ρ, with deposition temperature, T_{dep}.

3.2.2 Determination of activation energy

The dc conduction mechanism in many transition metal oxides above room temperature takes place by band conduction, where carriers excite beyond mobility edges into non-localized states, dominating the transport. The temperature dependence of electrical conductivity is of Arrhenius type and is expressed as

$$\rho = \rho_0 exp(E_a/KT) \quad (5)$$

Where ρ_0 is a pre-exponential factor, E_a is the activation energy for DC conduction, K is the Boltzmann's constant (8.617x 10-5 eV/k), and T is the absolute temperature. The dependence of deposition temperature on dc dark resistivity of WO_3 thin films is shown in Figure(6). The plots of $Ln\rho$ versus 1000/T at different deposition temperatures, T_{dep}, were found to be line indicating that conduction is performed through an activated process having two activation energies at different temperature regions. This is attributed to the thermally assisted hopping of carriers between localized states closes to Fermi level [30]. The values of ρ_0 and Ea were given in table (2).

Figure(7) plots $Ln\rho$ versus 1000/T as a function of annealing temperature which indicates that annealing change the line to have single activation energy. ρ_0 and Ea were given in table (3). It is inferred from the table that the obtained values of activation energy for the sample are ranged from 0.79-0.89 depending on the annealing process. These values of Ea are in good agreement with the data obtained by other workers [7,31,32].

© 2015 NSP
Natural Sciences Publishing Cor.

Table 2: dependence of activation energy on T_{dep}.

T_{dep} °C	$\rho_0(\Omega cm)$	$E_{\alpha 1}(eV)$	$E_{\alpha 2}(eV)$
250	$1.09x10^5$	0.70	0.62
300	$3.86x10^4$	0.76	0.38
350	$3.54x10^4$	0.72	0.48
400	$1.39x10^5$	0.79	0.22

Table 3: dependence of activation energy on T_{ann}.

T_{dep} °C	$\rho_0(\Omega cm)$	$E_{\alpha 1}(eV)$	$E_{\alpha 2}(eV)$
As-deposited	$1.38x10^5$	0.79	0.22
350	$3.25x10^4$	0.81	-
450	$5.54x10^4$	0.89	-
550	$7.40x10^4$	0.79	-

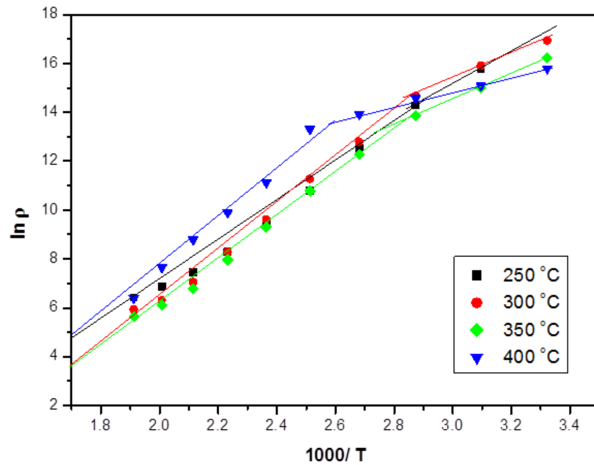

Fig. 6: plots of $ln\rho$ versus 1000/T, for samples prepared at different T_{dep}.

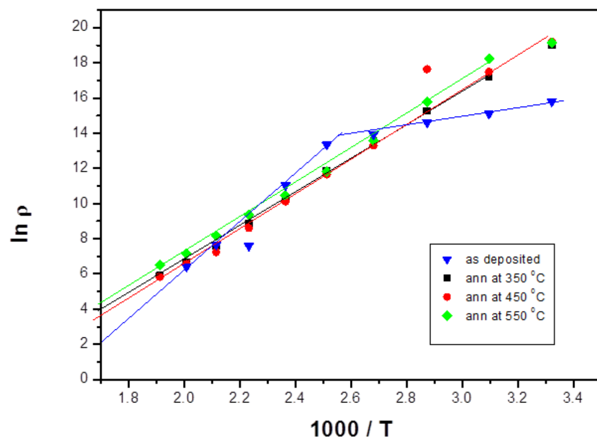

Fig. 7: plots of $ln\rho$ versus 1000/T, for sample annealed at different Tann. T_{ann}.

4 Conclusions

WO_3 films have been deposited from ammonium Para tungstate aqueous solution onto preheated glass substrate by spray pyrolysis technique at different deposition temperatures, T_{dep}. Microstructure and electrical properties have been experimentally characterized for the as grown samples as well as after annealing. The results show that the structure was amorphous for all samples deposited at T_{dep} = 250, 300, 350°C, while at T_{dep} = 400°C, the films were transformed to polycrystalline phase of WO3 with a hexagonal structure. Sample grown at a deposition temperature of 400°C was subjected to post-deposition annealing at different annealing temperatures (T_{ann}). An increase in the peak intensity is obtained and excess of peaks appeared with increasing T_{ann}. A decrease of the resistivity value is noticed with increasing deposition temperature (T_{dep}). The value of resistivity was found to be varied from $8.669x10^7 to 7.196x10_6 \Omega$.cm when T_{dep} varies from 250 to 400°C, respectively. The value of activation was found to be dependent on annealing process. The deposited sample possess two activation regions, however the annealed sample have only one activation energy. The activation energy values for the annealed sample were found to be around 0.89 eve for sample prepared at T_{dep} = 400°C and annealed at450°C.

References

[1] C.N.R. Rao, B. Raveau, Transition Metal Oxides, second ed., Wiley, New York, 1995, p. 4.

[2] S.K. Deb, *Philosophical Magazine* 27, 801-822 (1973).

[3] A.I. Gavrilyuk, *Electrochimica Acta* 44, 3027- 3037(1999). **24**,3027-3037, (1999).

[4] P. Jin, S. Nakao, S. Tanemura, Thin Solid Films 324, 151-153 (1998).

[5] P.K. Biswas, N.C. Pramanik, M.K. Mahapatra, D. Ganguli, J. Livage. *Materials Letters* 57, 4429-4432 (2003).

[6] A. Agrawal, J.P. Cronin, R. Zhang, *Solar Energy Materials and Solar Cells* 31, 9-21 (1993).

[7] A.A. Akl, H. Kamal, K. Abdel-Hady, *Physica B: Condensed Matter*, **325**, 65-75, (2003).

[8] M. Deepa, T.K. Saxena, D.P. Singh, K.N. Sood, S.A. Agnihotry, *Electrochimica Acta*, **10**, 1974-1989, (2006).

[9] C.G. Granqvist, A. Azens, L. Kullman, D. Ronnow, *Renewable energy*, **8**, 97-106, (1996).

[10] Z. Dimitrova, D. Gogova, *Materials Research Bulletin* , **40**, 333340, (2005).

[11] C. Cantalini, W. Wlodarski, Y. Li, M. Passacantando, S. Santucci, E. Comini, G. Faglia, G. Sberveglieri,*Sensors and Actuators B: Chemical*, **64**, 182-188,(2000).

[12] K. Galatsis, Y.X. Li, W. Wlodarski, K. Kalantar-zadeh, *Sensors and Actuators B: Chemical*, **77**, 478-483, (2001).

[13] D.S. Lee, K.H. Nam, D.D. Lee, *Thin Solid Films*, **375**, 142-146, (2000).

© 2015 NSP
Natural Sciences Publishing Cor.

[14] B. Fruhberger,M. Grunze, D.J. Dwyer, *Sensors and Actuators B: Chemical* , **31**,167-174 (1996).
[15] P.J. Shaver, *Applied Physics Letter*, **11**, 255-257,(1967).
[16] G.N. Chaudhari, A.M. Bende, A.B. Bodade, S.S. Patil, V.S. Sapkal, *Sensors and Actuators B: Chemical*, **115**, 297-302, (2006).
[17] Y.Wang, Z. Chen, Y. Li, Z. Zhou, X. Wu, *Solid-State Electron*, **45**, 639644, (2001).
[18] W. Qu and W. Wlodarski, ,*Sensors and Actuators B: Chemical*, **64**, 42-46, (2000).
[19] Y.-K. Chung, M.-H. Kim, W.-S. Um, H.-S. Lee, J.-K. Song, S.-Ch. Choi, K.-M. Yi, M. J. Lee and K. W. Chung, *Sensors and Actuators B: Chemical*, **60**, 49-55, (1999).
[20] S. H. Lee et al., *Journal of Applied Physics*, **88**, 3076-3078, (2000).
[21] R. Azimirad, O. Akhavan and A. Z. Moshfegh,*Journal of Electrochemical Society* , **153**, 49-55, (2006).
[22] J. Hao, S. A. Studenikin and M. Cocivera, *Journal of Applied Physics*, **90**, 5064-5072,(2001).
[23] S. A. Aly, *Defect and Diffusion Forum*,**11**, 295-296 (2009).
[24] E. Gyuorgy, G. Socol, I. N. Mihailescu, C. Ducu and S. Ciuca, *Journal of Applied Physics*, **97**, 1112911135, (2005).
[25] G. Garcia-Belmonte, P. R. Bueno, F. Fabregat-Santiago and J.Bisquert,*Journal of Applied Physics*,**96**, 853-861, (2004).
[26] M. Seman and C. A. Wolden, *Journal of Vacuum Science and Technology A*, **21**, 1927, (2003).
[27] S. A. Mahmoud. A. Mahmoud, *Solid State Sciences*, **4**,221-228, (2002).
[28] H.P.Klug and L.E. Alexander, *X-ray Diffraction Procedures*, Wiley, New York, (1954).
[29] A. Georg, W. Graf and V. Wittwer, *Solar Energy Materials and Solar Cells*, **51**,353-358, (1998).
[30] R. Sanjines, A. Aruchamy, and F. Levy, *Solid State Communications*, **64**, 645-655, (1987).
[31] M.C. Rao and O.M. Hussain, *Research Journal of Chemical Science* , **7**, 92-95, (2011).
[32] H. Kaneko, K. Miyake and Y. Teramoto, *Journal of Applied Physics*, **53**, 4416-4421 , (1982).

© 2015 NSP
Natural Sciences Publishing Cor.